AIAA JOURNAL
Vol. 44, No. 5, May 2006

Technical Notes

TECHNICAL NOTES are short manuscripts describing new developments or important results of a preliminary nature. These Notes should not exceed 2500 words (where a figure or table counts as 200 words). Following informal review by the Editors, they may be published within a few months of the date of receipt. Style requirements are the same as for regular contributions (see inside back cover).

Geometrical Description of Subgrid-Scale Stress Tensor Based on Euler Axis/Angle

Bing-Chen Wang* and Eugene Yee†
Defence Research and Development Canada–Suffield, Medicine Hat, Alberta T1A 8K6, Canada
and
Donald J. Bergstrom‡
University of Saskatchewan, Saskatoon, Saskatchewan S7N 5A9, Canada

I. Introduction

THE rotational dynamics between the fixed triads of two or more rigid bodies, or attitude dynamics,[1,2] is of fundamental interest to scientists and engineers working in the area of astronomy, spacecraft, satellites, and robotics. Recently, the methodology of attitude dynamics has been incorporated into fluids studies and provides some new insights into the local geometrical property of fluid tensors, construction of novel local structure-based constitutive relations for turbulence modelling,[3–5] and elucidation of the mechanism of a variety of physical processes such as dissipation and backscatter of the turbulence kinetic energy (TKE) between the resolved scale and subgrid-scale (SGS) motions.[6–10]

In the research areas related to rigid bodies, for example, maneuver of airplanes, motion of joints, and satellite control, there are multiple different and equivalent parameterization methods, each with its own merits and demerits, that can be used for investigating the attitude of a three-dimensional frame (or, in particular, the relative rotation of one frame with respect to another frame). Earlier milestones related to the topic of attitude dynamics include the famous work *Mécanique Analytique* by Joeseph-Louis Lagrange (1736–1813) and the quaternion introduced by Sir William R. Hamilton (1805–1865). Despite the long research history of the subject, modern advances and applications of the frame attitudes of rigid bodies still keep growing at an impressive rate in a number of diverse areas.[1,2,6–13] A fundamental difference in attitude representation between the area of fluid dynamics and those of astrodynamics,[12] aircraft engineering,[2,11] and robotic manipulation[13] is that the latter applications concern attitude control, whereas those in fluid dynamics have focused on the physical interpretation and computational consistency of the parameters of the representation.

Received 31 August 2005; revision received 7 December 2005; accepted for publication 14 December 2005.

*NSERC Visiting Fellow to Canadian Government Laboratory, P.O. Box 4000, Station Main; bingchen.wang@drdc-rddc.gc.ca.
†Defence Scientist, P.O. Box 4000, Station Main.
‡Professor, Department of Mechanical Engineering, 57 Campus Drive; don_bergstrom@engr.usask.ca.

Only two types of methods for attitude representation have, so far, been utilized in the literature of fluid dynamics. Betchov[14] pioneered the application of three Euler angles to study the geometrical properties of the velocity gradient tensor $u_{i,j} \overset{\text{def}}{=} \partial_j u_i$. This method was later systematically developed in Refs. 3–5 for investigation of the eigenframe attitude of the velocity gradient, Reynolds stress, SGS Reynolds stress, and SGS stress ($\tau_{ij} \overset{\text{def}}{=} \overline{u_i u_j} - \bar{u}_i \bar{u}_j$) tensors. Here, an overbar indicates a resolved/filtered quantity following the convention of large-eddy simulation (LES), and an eigenframe refers to an orthonormal triad formed by the three independent normalized eigenvectors of a second-order real symmetric tensor (such as τ_{ij}). For investigating the eigenframe attitude of $-\tau_{ij}$ with respect to the eigenframe of the resolved strain rate tensor [$\bar{S}_{ij} \overset{\text{def}}{=} (\bar{u}_{i,j} + \bar{u}_{j,i})/2$], Tao et al.,[9] Horiuti,[8] and Higgins et al.[10] adopted the axis-azimuth representation, which includes three angles, namely, the colatitude θ, longitude ϕ, and azimuthal angle ζ. (For details of the geometrical description, the readers are referred to the papers by Tao et al.[9] and Shuster.[11])

As just reviewed, to parameterize the attitude of the eigenframe of $-\tau_{ij}$ with respect to that of $\bar{S}_{ij}$, the conventional method is to use the Euler angles[3–5] or the axis-azimuthal angles.[8–10] However, note that the parameters used in both of these methods are not uniquely defined. The set of three Euler angles can be parameterized using in total 12 different equivalent ways (6 symmetric sets and 6 asymmetric sets) depending on the method that is adopted for decomposing the relative rotational motion between the two frames, and a similar situation holds for the axis-azimuth representation.[2,11] In this Technical Note, we propose a simple method to describe the attitude of the eigenframe of $-\tau_{ij}$ with respect to that of $\bar{S}_{ij}$, based on the Euler axis/angle. In contrast with the two mentioned methods of attitude parameterization through Euler angles and axis-azimuthal angles, the proposed method of Euler axis/angle is uniquely defined: It utilizes only one special angle, that is, Euler rotation angle χ, to quantify the rotation and only one special vector, that is, Euler axis $\boldsymbol{q}$ to define the central axis of the rotation. Both the Euler axis and Euler rotation angle are the so-called natural invariants[1] of the rotation matrix $\boldsymbol{R}$ and provide an elegant method for a simple decomposition and invariant representation of the relative rotation between two eigenframes through the use of Euler's theorem.

II. Rotational Motion in $\Re^3$ and Euler Axis/Angle

Let $\mathcal{E} = [\boldsymbol{e}_1, \boldsymbol{e}_2, \boldsymbol{e}_3]$ and $\mathcal{E}' = [\boldsymbol{e}'_1, \boldsymbol{e}'_2, \boldsymbol{e}'_3]$ be the basis vectors for the orthonormal observer-referenced frame (or the absolute frame) and the orthonormal object-referenced frame (or the relative frame), respectively. Let $\Re$ be the set of real numbers. The direction-cosine matrix $\boldsymbol{R} \in \Re^{3\times 3}$ is formed from the bases $\mathcal{E}$ and $\mathcal{E}'$ as

$$R_{ij} = \boldsymbol{e}'_i \cdot \boldsymbol{e}_j = \cos(\boldsymbol{e}'_i, \boldsymbol{e}_j) \tag{1}$$

which is referred to as the rotation matrix. This matrix links the frame $\mathcal{E}$ and $\mathcal{E}'$ through an orthogonal transformation. In consequence, we have

$$\boldsymbol{R}^T\boldsymbol{R} = \boldsymbol{R}\boldsymbol{R}^T = \boldsymbol{I}, \qquad \boldsymbol{R}^{-1} = \boldsymbol{R}^T, \qquad \det(\boldsymbol{R}) = \pm 1 \tag{2}$$

and $\boldsymbol{e}'_i = R_{ij}\boldsymbol{e}_j$ and $\boldsymbol{e}_i = R_{ji}\boldsymbol{e}'_j$. An orthogonal matrix corresponding to $\det(\boldsymbol{R}) = +1$ is called proper or special orthogonal (SO); otherwise, it is referred to as improper. A proper $\boldsymbol{R}$ represents pure

rotations, whereas an improper one involves reflections. More generally, we define the set of rotation matrices in n-dimensional space by

$$SO(n) = \{\boldsymbol{R} | \boldsymbol{R} \in \Re^{n\times n}, \boldsymbol{R}\boldsymbol{R}^T = \boldsymbol{I}, \det(\boldsymbol{R}) = +1\} \tag{3}$$

SO(3) corresponds to rotations in the three-dimensional space, which is usually referred to as the rotation group of $\Re^3$.

A rotation $\boldsymbol{R}$ can be directly used for representing the frame attitude; however, it has six redundant parameters. The proposed method of the Euler axis/angle representation is based on the famous Euler's theorem (see Refs. 1 and 13): Every rotation $\boldsymbol{R} \in SO(3)$ is equivalent to a rotation about a fixed axis $\boldsymbol{q}$ through an angle χ. Note that the fixed axis $\boldsymbol{q}$ (arbitrarily, using the normalized form, so that $|\boldsymbol{q}| = 1$) is not a free vector and is known as the Euler equivalent axis (or Euler axis for convenience). Euler's theorem implies that any arbitrary rotation between two rigid bodies can be uniquely defined by parameters $\boldsymbol{q}$ and χ, which are invariants of the rotation matrix $\boldsymbol{R}$ (or natural invariants[1]). Euler's theorem can be further understood from its eigensystem,[2] namely, $\boldsymbol{R}\boldsymbol{e} = \lambda\boldsymbol{e}$ with the characteristic equation

$$\det(\boldsymbol{R} - \lambda\boldsymbol{I}) = -\lambda^3 + \mathrm{tr}(\boldsymbol{R})\lambda^2 - \mathrm{tr}(\boldsymbol{R})\lambda + 1 = 0 \tag{4}$$

whose roots are the three eigenvalues of $\boldsymbol{R}$,

$$\lambda = +1, \qquad e^{i\chi}, \qquad e^{-i\chi} \tag{5}$$

where $i \overset{\text{def}}{=} \sqrt{-1}$. The Euler equivalent axis $\boldsymbol{q}$ corresponds to the eigenvector of the real eigenvalue $\lambda = +1$. However, χ, the Euler rotation angle is characterized by the phase of the other two eigenvalues. From Eq. (5), we obtain

$$\mathrm{tr}(\boldsymbol{R}) = \lambda_1 + \lambda_2 + \lambda_3 = 1 + 2\cos\chi \tag{6}$$

which determines the Euler rotation angle as $\chi = \cos^{-1}\{[\mathrm{tr}(\boldsymbol{R}) - 1]/2\}$. Furthermore, it can be shown[2] that the Euler axis $\boldsymbol{q} = [q_1, q_2, q_3]^T$ can be determined from the skew-symmetric part of $\boldsymbol{R}$ as

$$\boldsymbol{q}^\times = (\boldsymbol{R}^T - \boldsymbol{R})/(2\sin\chi) \tag{7}$$

where $\boldsymbol{q}^\times$ represents the following matrix:

$$\boldsymbol{q}^\times = \begin{bmatrix} 0 & -q_3 & q_2 \\ q_3 & 0 & -q_1 \\ -q_2 & q_1 & 0 \end{bmatrix} \tag{8}$$

Conversely, the rotation matrix $\boldsymbol{R}$ can also be calculated using the Euler axis/angle as

$$\boldsymbol{R} = \cos\chi\boldsymbol{I} + (1 - \cos\chi)\boldsymbol{q}\boldsymbol{q}^T - \sin\chi\boldsymbol{q}^\times \tag{9}$$

From Eq. (6), the Euler rotational angle χ can be determined from the trace of $\boldsymbol{R}$, and from Eq. (7), the Euler rotation axis can be determined provided that $\mathrm{tr}(\boldsymbol{R}) \neq +3$ or -1. If $\mathrm{tr}(\boldsymbol{R}) = 3$ or -1, the system becomes singular and the axis of rotation cannot be directly determined from Eq. (7). In the case of $\mathrm{tr}(\boldsymbol{R}) = 3$, $\boldsymbol{R} = \boldsymbol{I}$, $\boldsymbol{q}$ is not defined, and its direction is arbitrary. However, in the case that $\mathrm{tr}(\boldsymbol{R}) = -1$,

$$\boldsymbol{R} = 2\boldsymbol{q}\boldsymbol{q}^T - \boldsymbol{I} \tag{10}$$

from which $\boldsymbol{q}$ can be determined.

Figure 1 shows the geometry of the attitude of the eigenframe of $-\tau_{ij}$ with respect to that of $\bar{S}_{ij}$. Because both $-\tau_{ij}$ and $\bar{S}_{ij}$ are real and symmetric second-order tensors, they have three real eigenvalues that can be rearranged in a descending order, that is, $\alpha \geq \beta \geq \gamma$. The three orthonormal eigenvectors corresponding to these three eigenvalues are represented by $\boldsymbol{e}_\alpha$, $\boldsymbol{e}_\beta$ and $\boldsymbol{e}_\gamma$, respectively, which together in this sequence form an orthonormal right-handed triad. Because an eigenvector does not by itself contains any information regarding its direction, the elements of the rotation matrix $\boldsymbol{R}$ are evaluated using the absolute value of the direction cosines following

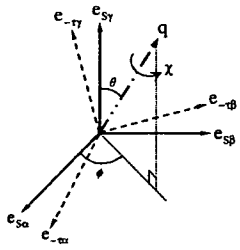

Fig. 1 Euler axis/angle describing the attitude of eigenframe of $-\tau_{ij}$ with respect to eigenframe of $\bar{S}_{ij}$.

the usual convention.[8–10] Note that although $-\tau_{ij}$ and $\bar{S}_{ij}$ are used as illustrative examples in this paper, the proposed method of Euler axis/angle representation is not specific to these two fluid tensors and can be used for investigation of other second-order real symmetric tensors with reference to an absolute or a relative frame.

III. Numerical Analysis

To demonstrate the proposed method of using the Euler axis/angle for studying the attitude of the eigenframe of the negative SGS stress tensor with respect to that of the resolved strain rate tensor, and also to examine the influence of near-wall anisotropy on the attitude of the eigenframe, numerical simulations have been performed using a turbulent Couette flow with a Reynolds number of 2600 (based on the channel width and one-half the velocity difference between the two plates). The physical domain used in the test was $8\pi\delta \times 2\delta \times 4\pi\delta$ along the streamwise x_1, wall-normal x_2, and spanwise x_3 directions. Here, δ is the half-channel width set to be 10 mm. The computational domain was discretized using 48^3 uniform control volumes. A second-order accurate finite volume code was used to perform the LES. For details of the numerical procedure and basic features of the flowfield, the reader is referred to Wang and Bergstrom.[6] Three dynamic SGS stress models were used in the simulations, namely, the conventional dynamic Smagorinsky model (DM) of Lilly[15]:

$$\tau_{ij}^*|_{\mathrm{DM}} = -2C_S\bar{\Delta}^2|\bar{S}|\bar{S}_{ij} \tag{11}$$

the dynamic two-parameter mixed model (DTPMM2) of Morinishi and Vasilyev[16]:

$$\tau_{ij}^*|_{\mathrm{DTPMM2}} = -2C_S\bar{\Delta}^2|\bar{S}|\bar{S}_{ij} + C_L\left(\overline{\bar{u}_i\bar{u}_j} - \bar{\bar{u}}_i\bar{\bar{u}}_j\right)^* \tag{12}$$

and the dynamic nonlinear model (DNM) of Wang and Bergstrom[6]:

$$\tau_{ij}^*|_{\mathrm{DNM}} = -2C_S\bar{\Delta}^2|\bar{S}|\bar{S}_{ij} - 4C_W\bar{\Delta}^2(\bar{S}_{ik}\bar{\Omega}_{kj} - \bar{\Omega}_{ik}\bar{S}_{kj}) - 4C_N\bar{\Delta}^2(\bar{S}_{ik}\bar{S}_{kj} - \bar{S}_{mn}\bar{S}_{nm}\delta_{ij}/3) \tag{13}$$

Here, an asterisk is used to indicate the trace-free form of a tensor, δ_{ij} is the Kronecker delta, $\bar{\Delta}$ is the grid-level filter size, $|\bar{S}| \overset{\text{def}}{=} (2\bar{S}_{mn}\bar{S}_{nm})^{1/2}$ is the norm of $\bar{S}_{ij}$, and $\bar{\Omega}_{ij} \overset{\text{def}}{=} (\bar{u}_{i,j} - \bar{u}_{j,i})/2$ is the rotation rate tensor. For description of the optimization procedure used to determine the preceding dynamic model coefficients C_S, C_L, C_W, and C_N, see the original literature.[6,15,16] The statistical results presented here are based on an average of 10,000 time steps. There are 30×30 bins used for calculating the two-dimensional joint probability density function (JPDF) and $20 \times 20 \times 20$ bins used for calculating the three-dimensional JPDF of the sample data in the homogeneous x_1–x_3 plane.

The set of unique natural invariant parameters $[\boldsymbol{q}, \chi]$ for quantifying the attitude of the eigenframe of $-\tau_{ij}$ with respect to that of $\bar{S}_{ij}$ is characteristic to a SGS model. For the same test condition, different models based on different constitutive relations are, in general, expected to be different in terms of the value of χ and the orientation of $\boldsymbol{q}$. Figure 2 shows the profile of the time- and plane-averaged Euler rotation angle χ across the channel in the wall-normal direction. The influence of wall anisotropy on the distribution of χ is evident in Fig. 2. In the core region of the channel, the value of χ predicted using the DNM is approximately 62 deg, which is slightly smaller than the approximate value of 69 deg predicted using the DTPMM2. The Euler rotation angle χ predicted using both the DNM and DTPMM2 decreases to 45 deg at the wall. Note that the proposed Euler rotation angle χ and Euler axis $\boldsymbol{q}$ are very effective in demonstrating

the degree of nonlinearity inherent in a SGS stress model and, thus, are useful in quantifying the difference between various SGS stress models.

For a linear model such as the DM of Lilly,[15] the constitutive relation for modeling the SGS stress takes the following form:

$$\tau_{ij} = f(\bar{S}_{ij}) \propto -\bar{S}_{ij}$$

which is qualitatively characterized by the singularity condition $\boldsymbol{R} \equiv \boldsymbol{I}$, $\chi \equiv 0$ deg, and the orientation of $\boldsymbol{q}$ being undefined. Because of the inclusion of the scale similarity term [associated with C_L in Eq. (12)] for the DTPMM2 and the inclusion of the two terms associated with C_W and C_N in Eq. (13) for the DNM, both the DTPMM2 and DNM deviate from the preceding linear constitutive relation. Consequently, for both the DTPMM2 and DNM, a rotation between the eigenframe of the modeled $-\tau_{ij}$ and that of $\bar{S}_{ij}$ exists in a general case, and consequently, the value of χ is expected to deviate from 0 deg, which in turn implies that $\boldsymbol{q}$ is well-defined through Eq. (7).

For this reason, the χ curves predicted using the DNM and DTPMM2 are distinctly different from that predicted using the DM as demonstrated in Fig. 2. From the demonstration, it is understood that the singularity condition is a signature of linearity for a SGS model indicating an exact parallel alignment between the principal axes of the modeled $-\tau_{ij}$ and those of $\bar{S}_{ij}$, whereas the inclusion of nonlinear components in the SGS stress model acts to "break" the singularity condition, resulting in a nonzero value of the Euler rotation angle χ and a well-defined Euler axis $\boldsymbol{q}$. As mentioned, it is also observed that near-wall anisotropy has a significant influence on the predicted values of χ both by the DNM and DTPMM2 (but not by the DM). This indicates that the degree of nonlinearity of a modeled SGS stress not only varies with the model constitutive relation, but also should vary with the distance from the wall (if the SGS stress is geometrically well modeled). For this reason, one really should not hope that a linear constitutive relation as represented by the DM is able to reflect correctly the tensorial geometrical nature of the SGS stress tensor for all of the different layers parallel to the wall in a wall-bounded flow.

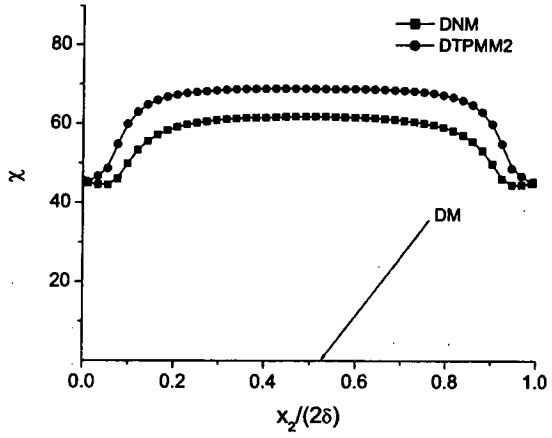

Fig. 2 Averaged profile for Euler rotational angle χ in wall-normal direction predicted by using three different dynamic SGS stress models.

To describe the Euler axis $\boldsymbol{q}$ (or the central axis of rotation of the eigenframe of $-\tau_{ij}$ with respect to that of $\bar{S}_{ij}$), we use the colatitude θ and longitude ϕ to describe its orientation (Fig. 1). When it is assumed that the orientation of the unit vector $\boldsymbol{q}$ is random in a three-dimensional Cartesian space, then on the surface of the unit sphere, the terminus of $\boldsymbol{q}$ is expected to be uniformly distributed in terms of the solid angle, which is defined as

$$S_\Sigma = \int\int_\Sigma \sin\theta \, d\theta \, d\phi \approx \sin\theta \cdot \Delta\theta \cdot \Delta\phi \tag{14}$$

where Σ is the area of the bin for statistics on the surface of the unit sphere. As demonstrated by Tao et al.[9] and Higgins et al.,[10] it is appropriate to evaluate the JPDF based on $\cos\theta$ and ϕ because it naturally includes the spherical effect through the solid angle, that is, $S_\Sigma \approx \sin\theta \cdot \Delta\theta \cdot \Delta\phi = -\Delta(\cos\theta) \cdot \Delta\phi$. Figures 3 and 4 show the JPDF of these two angles predicted using the DNM and DTPMM2, respectively. The JPDF value is calculated using the solid angle as the measure, that is, $(JPDF)_\Sigma = P_\Sigma / S_\Sigma$, and P_Σ is the probability corresponding to the bin Σ for a discrete system. From Fig. 3, it is observed that a state of $(\theta, \phi) = (66°, 0°)$ is the most probable for all three flow regimes: viscous sublayer, buffer layer, and logarithmic layer. As the wall is approached (x_2^+ decreases toward zero), the mode at $(66°, 0°)$ becomes more and more prominent. Figure 4 shows that the orientation pattern of $\boldsymbol{q}$ predicted using the DTPMM2 is, in general, similar to that predicted using the DNM, especially in the buffer layer and viscous sublayer. However, as shown in Fig. 4a,

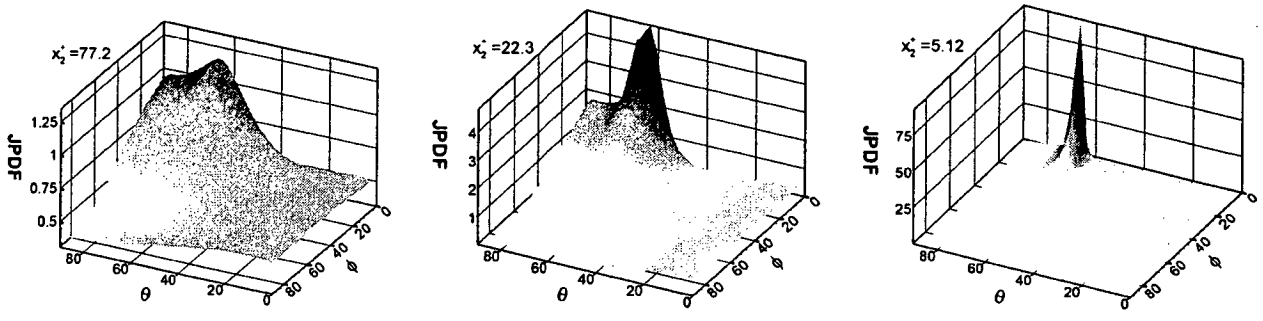

a) Logarithmic layer **b) Buffer layer** **c) Viscous sublayer**

Fig. 3 Two-dimensional JPDF of colatitude θ and longitude ϕ for specifying the random orientation of Euler axis q (predicted by using DNM).

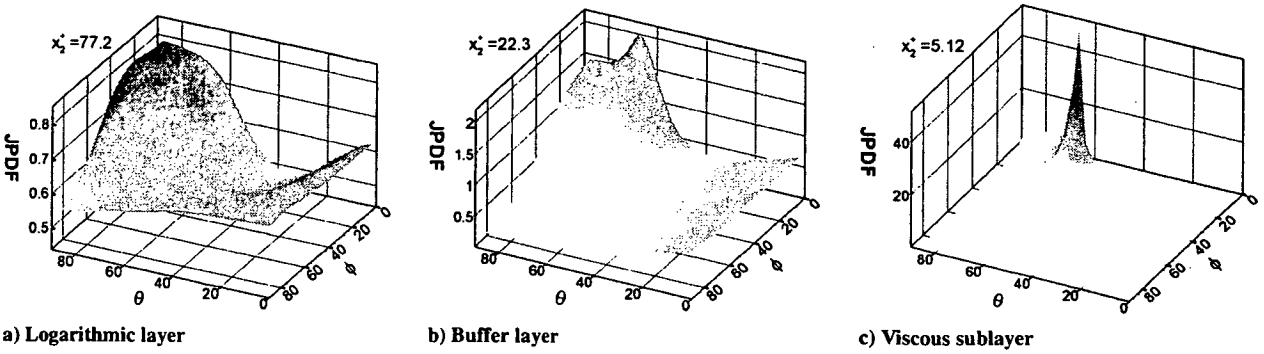

a) Logarithmic layer **b) Buffer layer** **c) Viscous sublayer**

Fig. 4 Two-dimensional JPDF of colatitude θ and longitude ϕ for specifying random orientation of Euler axis q (predicted by using DTPMM2).

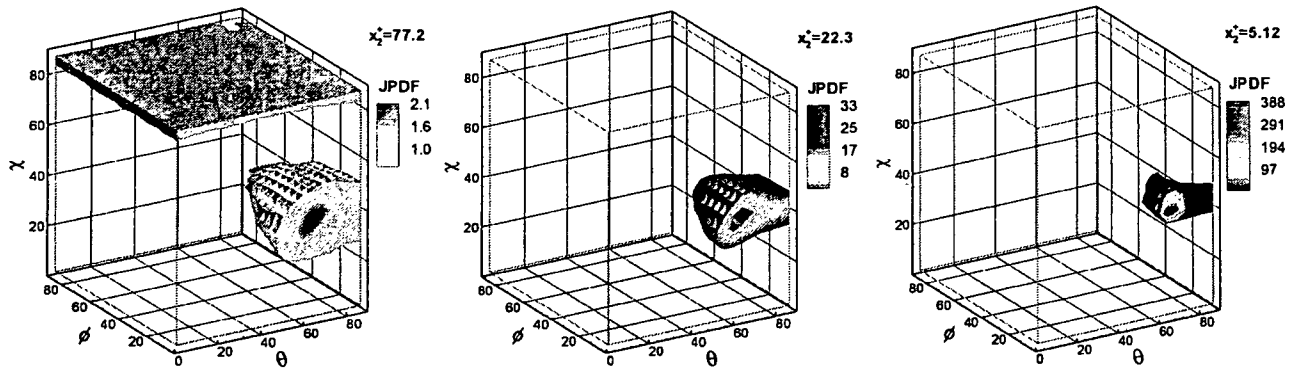

a) Logarithmic layer b) Buffer layer c) Viscous sublayer

Fig. 5 Three-dimensional JPDF of the Euler angle χ, colatitude θ, and longitude ϕ for describing random attitude of eigenframe of $-\tau_{ij}$ with respect to that of $\bar{S}_{ij}$ (predicted by using DNM).

although the state of $(\theta, \phi) = (66°, 0°)$ is still weakly preferred, the mode predicted by the DTPMM2 is broad, being distributed roughly in the region $(\theta, \phi) = (60\text{–}90°, 0\text{–}30°)$. Note that an uncertainty of $\pm 1.5°$ is inevitably involved in the analysis due to the finite number (30×30) of bins used in the calculation.

In the preceding discussion, we studied the Euler rotation angle χ and Euler axis $\boldsymbol{q}$ separately in Figs. 2–4. This is because both χ and $\boldsymbol{q}$ are physically meaningful quantities in the decomposition of the relative rotation between the two eigenframes of $-\tau_{ij}$ and $\bar{S}_{ij}$. It is of interest to understand the individual statistical behavior of χ and $\boldsymbol{q}$ as an independent random variable and vector, respectively. However, to investigate the general statistical property of random attitude of the eigenframe of $-\tau_{ij}$ with respect to eigenframe of $\bar{S}_{ij}$, it is also beneficial to examine the combined random system of $[\boldsymbol{q}, \chi]$, or equivalently the system of three independent random angles θ, ϕ, and χ. To keep the discussion brief, we only show in Fig. 5 the three-dimensional JPDF of θ, ϕ, and χ obtained using the DNM. To show clearly the most probable state, contours corresponding to very lower probabilities are clipped from Fig. 5. From Fig. 5, it is observed that for all three different flow regimes, there is a common predominant mode that corresponds to $(\theta, \phi, \chi) = (66, 0, 44 \text{ deg})$. In conformance with Fig. 3, it is evident from Figs. 5a–5c that the near-wall anisotropy also has a significant impact on the three-dimensional JPDF levels. As the wall is approached, this mode at $(\theta, \phi, \chi) = (66, 0, 44 \text{ deg})$ becomes more and more prominent. As shown in Fig. 5a, in the logarithmic layer, there exists a secondary mode that corresponds to $\chi = 90$ deg with θ and ϕ arbitrary. The near-wall anisotropic effect on the three-dimensional JPDF pattern as exhibited in Figs. 5a–5c, explains the characteristic of the plane-averaged profile of χ as demonstrated in Fig. 2, namely, the plane-averaged value of χ is the smallest (45 deg) at the wall and increases to its maximum (62 deg) at the center of the channel. Note that because only $20 \times 20 \times 20$ bins were used for calculating the three-dimensional JPDF, an uncertainty of ± 2.25 deg exists in the preceding analysis.

IV. Conclusions

In comparison with previous methods for parameterizing the relative rotation between the eigenframes of $-\tau_{ij}$ and $\bar{S}_{ij}$, we believe that the proposed Euler axis/angle presents a method for describing the attitude of the eigenframe of $-\tau_{ij}$ with respect to that of $\bar{S}_{ij}$ in a simple and unique manner. This method is based on classical Euler's theorem and utilizes only one special angle, that is, Euler rotation angle χ, to quantify the relative rotation between two frames and only one special vector, that is, Euler axis $\boldsymbol{q}$, to define the central axis of the rotation, both of which are the natural invariants of the rotation matrix $\boldsymbol{R}$. Both the Euler rotation angle χ and Euler axis $\boldsymbol{q}$ were found to be very effective in demonstrating the difference between the SGS stress models in terms of their degree of nonlinearity. For the classical DM of Lilly,[15] which is based on a linear constitutive relation between $-\tau_{ij}$ and $\bar{S}_{ij}$, the Euler rotation angle $\chi \equiv 0$ deg and the Euler axis $\boldsymbol{q}$ is undefined corresponding to a singular condition. In contrast, due to nonlinearity, the averaged Euler rotation angle χ predicted using the DNM and DTPMM2 deviates from 0 deg, ranging instead from 62 to 69 deg in the core region of the channel and deceasing to 45 deg at the wall. To quantify the orientation the Euler axis $\boldsymbol{q}$, the colatitude θ and longitude ϕ were used. It is found in the simulations that the presence of the walls has a strong anisotropic effect on the orientation of $\boldsymbol{q}$. The two-dimensional JPDF of θ and ϕ predicted using both the DNM and DTPMM2 has a mode at $(\theta, \phi) = (66°, 0°)$. This mode is prominent in the near-wall region, but corresponds to a much broader distribution in the core (logarithmic) flow regime. Similarly, the three-dimensional JPDF mode of $(\theta, \phi, \chi) = (66, 0, 44 \text{ deg})$ predicted by the DNM is the most strongly expressed in the viscous sublayer. In the logarithmic layer, a secondary mode for the three-dimensional JPDF at $\chi = 90$ deg with θ and ϕ being arbitrary is also observed, which is consistent with the observation that the time- and plane-averaged value of χ is the largest in center of channel and is the smallest at the wall.

Note that at this stage no data are available in the literature for comparison with the current preliminary numerical results obtained using the a posteriori LES method. In future studies, it is of interest to further explore the proposed method for quantification of the degree of nonlinearity of other SGS stress models and for investigation of the forward and backward scatter of TKE between different scales of motions. Also, it is important to extend the proposed method to a priori LES studies using experimental or direct numerical simulation data.

Note that, in this paper, we study only the relative rotation of the eigenframe of $-\tau_{ij}$ with respect to that of $\bar{S}_{ij}$. However, the proposed method of the Euler axis/angle representation is also applicable for studying any second-order real symmetric fluid tensor in term of its eigenframe attitude relative to either an absolute coordinate system or the eigenframe of another tensor. In an a priori LES test, the most desirable scenario is to have the principal axes of the modeled τ_{ij} aligned with those of the measured τ_{ij}, in which case, the SGS stress model is considered to conform well with the geometrical property of the actual SGS stress tensor. For this case, the relative rotation of the eigenframe of the modeled τ_{ij} with respect to that of the measured τ_{ij} degenerates to a singularity condition, which is also characterized by a parallel alignment between the principal axes of the two tensors, corresponding to $\boldsymbol{R} \to \boldsymbol{I}$ and $\chi \to 0$ deg. (Here, $\boldsymbol{R}$ and χ are due to the relative rotation between the two orthonormal eigenframes of the modeled and measured τ_{ij}.)

Acknowledgments

Support from the National Sciences and Engineering Research Council as a visiting fellowship to B. C. Wang and a research grant to D. J. Bergstrom is gratefully acknowledged. The authors thank FangXiang Wu for beneficial discussions regarding the geometrical property of a tensorial eigensystem.

References

[1] Angeles, J., *Rational Kinematics, Springer Tracts in Natural Philosophy*, Vol. 34, Springer-Verlag, New York, 1988, Chaps. 1–3.

[2]Hughes, P. C., *Spacecraft Attitude Dynamics*, Wiley, New York, 1986, Chaps. 1–3.

[3]Saffman, P. G., and Pullin, D. I., "Anisotropy of the Lundgren–Townsend Model of Fine-Scale Turbulence," *Physics of Fluids*, Vol. 6, No. 2, 1994, pp. 802–807.

[4]Pullin, D. I., and Saffman, P. G., "Reynolds Stresses and One-Dimensional Spectra for a Vortex Model of Homogeneous Anisotropic Turbulence," *Physics of Fluids*, Vol. 6, No. 5, 1994, pp. 1787–1796.

[5]Misra, A., and Pullin, D. I., "A Vortex-Based Subgrid Stress Model for Large-Eddy Simulation," *Physics of Fluids*, Vol. 9, No. 8, 1997, pp. 2443–2454.

[6]Wang, B.-C., and Bergstrom, D. J., "A Dynamic Nonlinear Subgrid-Scale Stress Model," *Physics of Fluids*, Vol. 17, No. 3, 2005, 035109.

[7]Wang, B.-C., Yin, J., Yee, E., and Bergstrom, D. J., "Turbulence Topologies Predicted Using a Dynamic Non-Linear Subgrid-Scale Model Based on Speziale's Quadratic Constitutive Relation," *4th International Symposium on Turbulence and Shear Flow Phenomena*, 2005, pp. 1055–1060.

[8]Horiuti, K., "Roles of Non-Aligned Eigenvectors of Strain-Rate and Subgrid-Scale Stress Tensors in Turbulence Generation," *Journal of Fluid Mechanics*, Vol. 491, 2003, pp. 65–100.

[9]Tao, B., Katz, J., and Meneveau, C., "Statistical Geometry of Subgrid-Scale Stresses Determined from Holographic Particle Image Velocimetry Measurements," *Journal of Fluid Mechanics*, Vol. 457, 2002, pp. 35–78.

[10]Higgins, C. W., Parlange, M. B., and Meneveau, C., "Energy Dissipation in Large-Eddy Simulation: Dependence on Flow Structure and Effects of Eigenvector Alignments," *Atmospheric Turbulence and Mesoscale Meteorology: Scientific Research Inspired by Douglas K. Lilly*, edited by E. Fedorovich, R. Rotunno, and B. Stevens, Cambridge Univ. Press, Cambridge, England, U.K., 2004, pp. 51–69.

[11]Shuster, M. D., "A Survey of Attitude Representations," *Journal of the Astronautical Sciences*, Vol. 41, No. 4, 1993, pp. 439–517.

[12]Battin, R. H., *An Introduction to the Mathematics and Methods of Astrodynamics*, rev. ed., AIAA Education Series, Springer, New York, 1999.

[13]Murray, R. M., Li, Z., and Sastry, S. S., *A Mathematical Introduction to Robotic Manipulation*, CRC Press, Boca Raton, FL, 1994, Chaps. 1–3.

[14]Betchov, R., "An Inequality Concerning the Production of Vorticity in Isotropic Turbulence," *Journal of Fluid Mechanics*, Vol. 1, 1956, pp. 497–504.

[15]Lilly, D. K., "A Proposed Modification of the Germano Subgrid-Scale Closure Method," *Physics of Fluids A*, Vol. 4, No. 3, 1992, pp. 633–635.

[16]Morinishi, Y., and Vasilyev, O. V., "A Recommended Modification to the Dynamic Two-Parameter Mixed Subgrid Scale Model for Large Eddy Simulation of Wall Bounded Turbulent Flow," *Physics of Fluids*, Vol. 13, No. 11, 2001, pp. 3400–3410.

P. Givi
Associate Editor